Small-polaron coherent conduction in lightly doped ReTiO$_{3+\delta/2}$ (Re=La or Nd) thin films prepared by Pulsed Laser Deposition

J. Li,[1,][*] F. B. Wang,[1,][2] P. Wang,[1] M. J. Zhang,[1] H. Y. Tian,[1] and D. N. Zheng[1]

[1]*National Laboratory for Superconductivity, Beijing National Laboratory for Condensed Matter Physics and Institute of Physics, Chinese Academy of Sciences, Beijing 100080, China.*
[2]*Sichuan University, College of Materials Science & Engineering, Chengdu 610064, China*
(Dated: February 6, 2008)

LaTiO$_{3+\delta/2}$, NdTiO$_{3+\delta/2}$, and Nd$_{1-x}$Sr$_x$TiO$_{3+\delta/2}$ thin films have been epitaxially grown on (100)SrTiO$_3$ and (100)LaAlO$_3$ single crystal substrates by using the pulsed laser deposition technique. The oxygen pressure during deposition has been carefully controlled to ensure that the films are lightly doped in the metal side near the metal-Mott-insulator boundary. A steep drop of the effective carrier number at low temperatures has been observed in some of the films, which may correspond to a gradually opening of the Spin Density Wave (SDW) gap due to the antiferromagnetic spin fluctuations. At elevated temperatures, a thermally induced decrease of the Hall coefficient can also be clearly observed. In spite of the fact that these films were prepared from different materials in varied deposition conditions, the temperature dependence of their resistance can all be almost perfectly fitted by a small-polaron coherent conduction model ($R_s(T) = R_s(0) + C\omega_\alpha/\sinh^2(T_\omega/T)$). Careful investigation on the fitting parameters implies that the frequency of the phonon coupled to the electrons may be partially related to the lattice distortion induced by the mismatch strain of the substrates.

I. INTRODUCTION

The titanates ReTiO$_3$ (where Re is a trivalent rare-earth ions) are canonical Mott-Hubbard type insulators with Ti^{3+} ($3d^1$ t_{2g}) electron configuration.[1] It has been widely accepted that the insulating behavior is ascribed to the strong Coulomb repulsion among the integer number of electrons at each Ti sites, which opens a charge gap at the Fermi surface. The gap width is determined by the electron correlation strength, U/W, where U is the on-site Coulomb energy and W is the one-electron bandwidth. Varying the GdFeO$_3$-type distortion by changing the radius of Re ions or by applying an external hydrostatic pressure, one can tune the bandwidth W and hence the correlation strength. A bandwidth-controlled insulator-metal transition then can occur. Alternatively, anomalous metallic states can also be derived from the Mott insulators upon carrier doping, by substituting the trivalent rare-earth with a divalent ion or by introducing excess oxygen atoms into the lattice, the so-called filling-controlled insulator-metal transition.

Generally speaking, the pure perovskite ReTiO$_3$ (Ti^{3+}, $3d^1$) crystals with a stoichiometric oxygen content can only be acquired in an extremely reducing atmosphere.[2,3] The Ti oxides have a strong tendency to incorporate La and Ti vacancies, which are frequently denoted by an excess of oxygen in the formula, ReTiO$_{3+\delta/2}$.[4] With the increase of nominal hole doping δ, the material evolves from a Mott insulator with a spin and orbital ordering, to a paramagnetic metal of filling level $1 - \delta$ in the $3d$ band. As δ is larger than 0.4, the effective carrier density in the system decreases,

and additional oxygen layers appear along the perovskite {110} planes. The end member ReTiO$_{3.5}$ is a band insulator (Ti^{4+}, $3d^0$) with a layer-perovskite structure, which becomes ferroelectric at an enormously high transition temperature.[5]

The electronic properties of the Ti oxides in the vicinity of the metal-Mott-insulator transition have been widely studied during the past decade. A striking quadratic temperature dependence (T^2) of resistivity has been conspicuously observed over a large temperature range in the metallic LaTiO$_{3+\delta}$[3] and Sr-substituted Sr$_{1-x}$La$_x$TiO$_{3+\delta}$[6] single crystals, accompanied by a remarkable electron effective mass enhancement. This had been attributed to the strong electron-electron correlation in the system. Other characteristic properties, such as temperature independent Pauli-like susceptibility and the T-linear electronic specific heat are also discovered, the doped titanium oxides were then argued to be well described by the Fermi liquid picture.

Nevertheless, in contrast to the comprehensive investigations on single crystal samples, reports on titanate thin films[7,8,9,10] are limited in quantity and the analyses are somewhat at a superficial level. Hwang *et al.*[7] has demonstrated that, up to 6 unit-cell-thick LaTiO$_3$ layers can be stabilized on SrTiO$_3$ substrate at conventional deposition conditions. As the film grows thicker, however, a high density of {110} faults (excess oxygen layers inserted) will develop, driven energetically to achieve the equilibrium oxidative state of Ti. Accordingly most of the films prepared in reduced oxygen pressures behave metallically, although a diversity in the absolute resistivity value and the temperature dependency was noticed.

Among the few attempts to model the metallic transport properties in titanate thin films, Gariglio *et al.*[10] was very successful by considering the interaction between electrons and phonons.

In this experiment, we deposited epitaxial thin films of different titanates on both $(100)SrTiO_3$ (STO) and $(100)LaAlO_3$ (LAO) single crystal substrates at varied temperatures and low oxygen pressures. We are surprised to find that, the temperature dependencies of the film resistivity can all be excellently fitted by a small-polaron coherent conduction model[10,11].

II. EXPERIMENT

The $LaTiO_{3+\delta/2}$ (LTO) and $NdTiO_{3+\delta/2}$ (NTO) thin films have been grown on STO and LAO substrates by using the pulsed laser deposition (PLD) technique in a high vacuum chamber. The ceramic $LaTiO_{3.5}$ and $NdTiO_{3.5}$ targets were fabricated by conventional solid-state reaction at $1370\,^\circ$C and $1400\,^\circ$C, respectively, in air or flowing oxygen for 10 hours. The Sr doped NTO film was prepared by sticking a small piece of STO single crystal onto the ceramic NTO target. A KrF excimer laser with 248 nm wavelength was employed for ablation. The substrate temperature was within 650 to $850\,^\circ$C, and the laser energy density was around 2 J/cm^2. Most of the films were deposited in the background vacuum (BV) below 5×10^{-4} Pa, whereas a few were prepared in slightly higher oxygen pressures. The deposition lasted for 30 minutes with a laser repetition rate of 2 Hz. After growth the films were annealed *in situ* for 10 minutes at the deposition temperature and oxygen pressure, and then cooled down to room temperature in a ramp rate of $40\,^\circ$C/min. The thickness of the films is estimated to be $\sim$2000 Å.

The crystal structure of these films was monitored *in situ* by a reflection high-energy electron diffraction (RHEED) system, and studied *ex situ* by x-ray diffraction. The electrical resistivity and Hall coefficient were measured using the van der Pauw geometry (5×5mm^2) in the temperature range 5 K$<$ T $<$300 K. The electrical contacts were made by indium soldering. Magnetization measurements were carried out by first cooling the samples down to 5 K in a 5 T magnetic field, and then measuring in a warming run in 100 Oe. The Hall measurements were carried out in an MPMS superconducting quantum interference (SQUID) measuring system and a Maglab multipurpose magnetic measuring system.

III. RESULTS AND DISCUSSIONS

All the films prepared are epitaxial, with excellent in-plane and out-of-plane orientations. Shown in Fig. 1 is a typical XRD θ-2θ spectrum for an NTO thin film deposited on an LAO substrate at $650\,^\circ$C in vacuum. No impurity phase can be identified. The rocking curve of NTO[001]$_c$ is inserted, whose FWHM is $\sim$1°. The
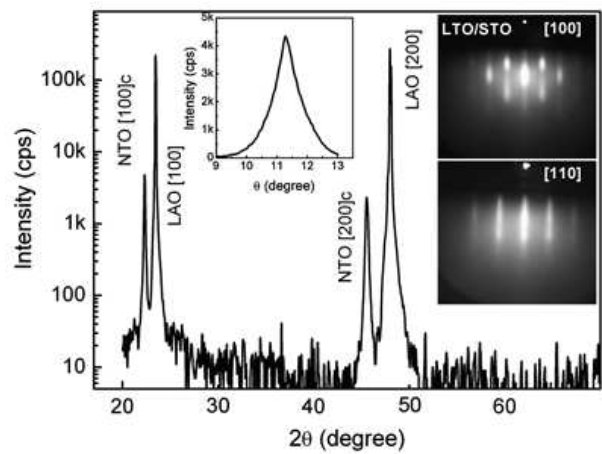

FIG. 1: XRD θ-2θ spectrum for film NTO/LAO grown at $650\,^\circ$C in vacuum. The inset is the rocking curve of NTO[001]$_C$. The $<100>$ and $<110>$ RHEED images for film LTO/STO grown at $850\,^\circ$C in vacuum is also inserted.

XRD reflections for the films grown on STO cannot be resolved from the substrate peaks due to the very close lattice constants. Thereby, the RHEED images for an LTO thin film grown on an STO substrate at $850\,^\circ$C in vaccum is shown instead, taken along the $<100>$ and $<110>$ zone-axes. The film was grown in a cube-on-cube way, with its pseudo-cubic perovskite {001} planes parallel to the film surface. The diffraction streaks are bright and sharp, suggesting a good crystallinity of the film. RHEED images for films on LAO substrates show almost no dissimilarity. Some of the films, especially the NTO films, exhibit a superstructure of $2a_0$ (a_0 is the lattice constant of the cubic perovskite structure) in their RHEED diffraction patterns. This is most probably due to the GdFeO$_3$-type distortion of the perovskite lattice.

The films deposited in the background vacuum or slightly higher oxygen pressures, say 10^{-3} Pa, all behave like a metal from room temperature to 5 K. Some shows a small resistivity upturn at low temperatures, while the others do not unto 5 K. In Fig. 2 we plot the *sheet* resistance R_s versus T^2 curves for these films. It is noticed that, although some of these samples have resistance one or two orders of magnitude higher than the others, these curves are similar in two ways: (a) in high temperature regions, the resistance shows an approximately linear dependence on T^2. (b) at a low temperature T^*, however, the resistance starts to deviate visibly from this law and goes up, as can be clearly seen in the inset, no matter if there is an upturn or not in the $R - T$ curves. T^* ranges from 120 K to 200 K or even higher. The T^2 dependence of resistivity ($\rho = \rho_0 + AT^2$) has long been observed in transition metals[12], and later in doped V_2O_3[13] and titanate single crystals[3]. It has been attributed to the strong electron-electron correlations in these systems. The coefficient A in transition metal Iron, Nickel and Cobalt is in the order of $10^{-11}\Omega$ cmK^{-2}, and that in the doped V_2O_3 is $5\times10^{-8}\Omega$ cmK^{-2}. The A values in
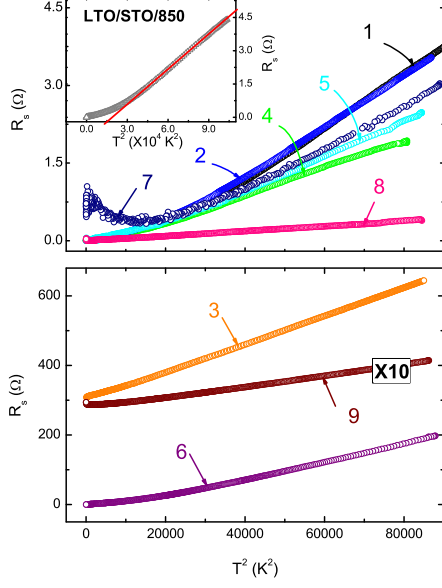
FIG. 2: (Color online) R_s versus T^2 curves for the various lightly-doped epitaxial thin films deposited. The sample details are listed in Table I.

FIG. 3: The $R_s - T$ and $n_s - T$ curves for an NTO thin film grown on an STO substrate at $850\,^{\circ}$C in vacuum.

FIG. 4: The $R_s - T$ and $n_s - T$ curves for an Sr doped NTO thin film grown on an LAO substrate at $850\,^{\circ}$C in vacuum. The dash line denotes the M-I transition temperature.

our experiment are determined to be between $9\times10^{-11}\Omega$ cmK^{-2} and $8\times10^{-8}\Omega$ cmK^{-2}, comparable to the previous results. Nevertheless, in the strong correlation frame, the T^2 dependence is usually dominant at low temperatures. A phonon scattering term shows up only as temperature increases. Apparently, our data disagree with this rule, suggesting that the conduction mechanism of epitaxial thin films may somewhat differ from that of the single crystals.

On the other hand, while most of the previous studies reported temperature-independent carrier density, which is a character of Fermi liquid, our measurements demonstrate a clear temperature variation of the Hall coefficient. In Fig. 3, we show the $R_s - T$ curve for the NTO thin film grown on an STO substrate at $850\,^{\circ}$C in a background vacuum. The sample represents the lowest resistivity we have ever reached. Assuming that the film thickness is 2000Å, its room temperature resistivity is approximately $6.1\mu\Omega$cm, and the value is only $4.2\times10^{-2}\mu\Omega$cm at 5 K. The Hall signal was measured in a perpendicular magnetic field scanned from -5T to +5T at fixed temperatures by using a Maglab-12 (Oxford). The field dependence of the crossover resistance R_{xy} was recorded. A typical $R_{xy} - H$ relationship is given in the inset of the figure, suggesting a negative carrier type. The *sheet* carrier density was read from the slope of these curves using the standard free carrier Hall effect formula $n_s = B/eR_{xy}$, and is also shown in the figure. The error bar was added according to the linear fitting errors, which are underestimated because the temperature fluctuations and the geometric irregular of
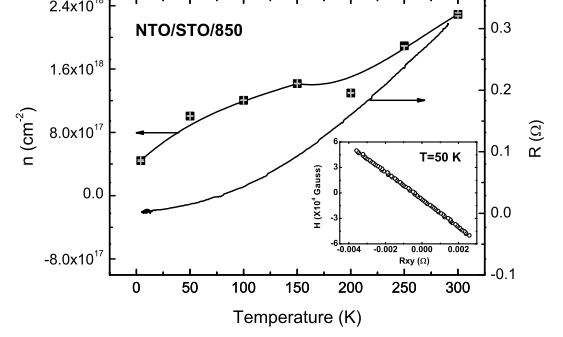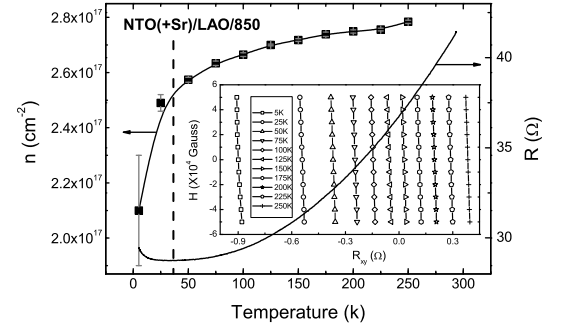
the sample are not considered. It is clear that, although the sample is a good metal throughout the whole temperature range measured, its carrier density decreases with decreasing temperature. The carrier density n is estimated to be from 2.2×10^{22}cm^{-3} to 1.1×10^{23}cm^{-3}, which is, however, unphysical since the highest n calculated by assuming one d electron per unit cell is only around 1.65×10^{22}cm^{-3}. The overestimated carrier density may be originated from experimental errors, or most probably from the simple free carrier assumption.

Shown in Fig. 4 is the Sr doped NTO on an LAO substrate at $850\,^{\circ}$C in a background vacuum. This sample shows a resistance two orders of magnitude higher and a clear M-I transition at $\sim$20 K. The Hall measurement for this sample was performed by a SQUID MPMS5 (Oxford), and also in a field of -5T to +5T. Because of the poor alignment of the voltage electrodes, the $R_xy - H$ curves measured are severely asymmetric for positive and negative fields, but the slopes of these curves are distinct, as can be seen in the inset. The derived carrier density decreases gradually with decreasing temperature, and drops steeply near the M-I transition point,

TABLE I:

No.	Sample	Denotation	P_O/BV (Pa)	$R_s(0)$ (Ω)	$C\omega_\alpha$ (Ω)	C ($10^{-14}\Omega\cdot S^{-1}$)	T_ω (K)	χ^2	R^2
1	260505	LTO/STO/850	5e-4	0.024(1)	4.47(4)	6.0	284.6(9)	0.00086	0.99952
2	120905	LTO/STO/650	4.3e-4	0.041(1)	3.49(3)	5.1	260.0(9)	0.00055	0.99959
3	230505	LTO/LAO/850[a]	5e-4	312.0(1)	38.8(9)	151.7	97.90(8)	1.67078	0.99989
4	111104	LTO/STO/780	4.5e-4	0.021(2)	0.85(2)	1.8	176.65(5)	0.00042	0.99905
5	191104	LTO/STO/650	5e-4	0.053(2)	1.78(4)	3.0	226.62(5)	0.00067	0.99907
6	140805	NTO/STO/850	6e-3	1.80(9)	143.1(7)	237.0	230.77(9)	1.89505	0.99923
7	121005	NTO/STO/650	5e-4	0.320(5)	7.0(2)	7.1	374.6(4)	0.00073	0.99897
8	120805	NTO/STO/850 [b]	6e-4	0.0016(1)	0.0005(4)	0.008	25.0(9)	1.0273e-6	0.998
9	241005	NTO(+Sr)/LAO/850	2.4e-4	28.798(3)	5.77(3)	11.8	186.3(5)	0.0011	0.99993

[a]This film can also be well fitted by the T^2 relationship.

[b]Fitting of this sample gives a low reliability.

resulting in the upturn of resistivity at low temperatures. Here we note that, for Sr doped NTO single crystals, the low temperature antiferromagnetism (AFM) survives until the doping level is higher than 0.2[14]. Strong antiferromagnetic fluctuations may persist well above T_N, which gradually opens a spin density wave (SDW) gap over some portion of the Fermi surface as the temperature is decreased[15]. We believe this is the reason for the effective carrier number collapse and the concomitant resistivity increase below 20 K. Inductively coupled plasma - atomic emission spectrometry (ICP-AES) reveals that, however, the La:Sr ratio in this sample is 1:0.93, which means that the filling level $1 - x - \delta$ should be around 0.5. Because of the substrate effect, as we will discuss later, AFM may still lingering in the sample, although the chemical analysis destroys the sample, making the magnetization measurement unavailable. The carrier density n is derived to be from 1.0×10^{22}cm^{-3} to 1.4×10^{22}cm^{-3}, while the ideal carrier density should be no more than 8.5×10^{21}cm^{-3}. Therefore, the derived carrier density in this sample is again overestimated.

Therefore, although the two samples show different transport behaviors, they all exhibit a thermally induced increase of the effective carrier number, which is inconsistent with the Fermi liquid picture. Considering our $R - T$ fitting results, as will be detailed below, we prefer to explain this phenomenon using a polaron conduction picture. A theory of small-polaron coherent conduction was developed in 1968 by Bogomolov et $al.$[16], and has been adopted by Zhao et $al.$[11] to explain the metallic transport behavior in the doped perovskite manganite thin films. Gariglio et $al.$[10] also found recently that this model could interpret well the conduction behavior of their LTO thin films grown on LAO substrates. In this model, the resistivity is given by

$$\rho(T) = \rho_0 + (\hbar^2/ne^2a^2t_p)\sum_\alpha A_\alpha\omega_\alpha/\sinh^2(\hbar\omega_\alpha/2k_BT),$$

where n is the carrier density, a is the lattice constant, t_p is the effective hopping integral of polarons, ω_α is the average frequency of one optical phonon mode, and A_α is a constant depending on the electron-phonon coupling strength. The fully activated heavy particles are scattered by thermal phonons and thus the resistivity increases with increasing temperature. Assuming that only the low-lying optical mode with a strong electron-phonon coupling contributes to the resistivity, we fit the $R - T$ curves shown in Fig. 2 using the expression

$$R_s(T) = R_s(0) + C\omega_\alpha/\sinh^2(T_\omega/T).$$

The fitting parameters are listed in Table I. The curve fittings were done without weighting. For the curves with an upturn at low temperatures, we fit only the data above the transition point. It is striking that the model can perfectly fit almost all of the experimental data in Fig. 2, in spit of the fact that these samples are made from different kinds of materials on both STO and LAO substrates at varied temperatures and in different oxygen pressures. Values of the $goodness$ of fit R^2 are all ≥ 0.999, except that for Sample 120805 (also shown in Fig. 3). R^2 for this sample is slightly lower, most probably due to its rather high single-to-noise ratio. Therefore the fitting result is ignored in the following analyses. The excellent agreement between the experimental and the calculated curves strongly implies the presence of small-polarons and their metallic conduction in the perovskite titanate thin films. The small fitting error may have its origin that, in the model the carrier density n is treated as a constant, while in fact it changes slowly with temperature.
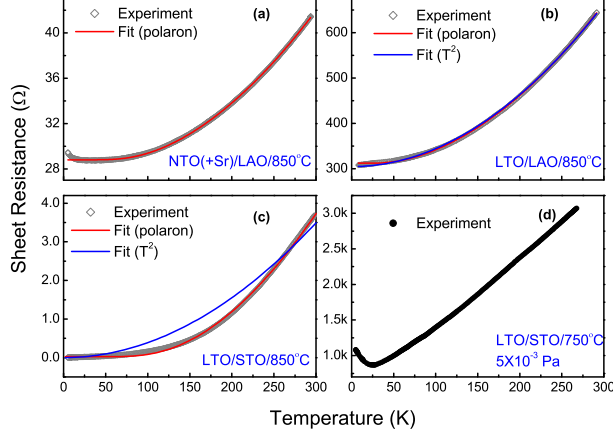
FIG. 5: (Color online) Examples of the small-polaron fitting results.

FIG. 6: Magnetization curves for some of the LTO and NTO thin films measured in a perpendicular magnetic field of 100 Oe (5T field-cooled)[14].

In Fig. 5(a), (b), and (c) we give three examples of the curve fittings. Fig. 5(a) is for curve 9 (sample 241005, also shown in Fig. 4). Fitting was performed only from 35 K to 295 K, but the calculated curve is extended to low temperatures in the figure. In Fig. 5(b) we show fitting for curve 3 (sample 230505) using both the T^2 relationship and the small-polaron model. This sample shows the best fitting result by the T^2 relationship among all the films prepared, even though the R^2 value for small-polaron is still larger. Curves for the other films presented in Fig. 2 can only be satisfactorily fitted by the polaron model, as illustrated in Fig. 5(c) (curve 9, sample 260505). Nevertheless, only the films with hole doping near the Mott-insulator-metal transition boundary can be well fitted by the small-polaron coherent conduction model. For thin films deposited in elevated oxygen pressures, as that shown in Fig. 5(d), though still behaves like a metal, at high temperatures the resistivity is remarkably enhanced and almost temperature linearly dependent. This sample corresponds to a highly oxygen-doped state far away from the I-M transition. With increasing of the oxygen pressure, extra oxygen layers gradually appear in the originally cubic perovskite lattice. The film then becomes a mixture of two-dimensional (2D) and three-dimensional (3D) regions. The linearly T-dependent behavior may suggest a kind of 2D conduction behavior, like in the case of high-temperature superconductor normal state[10].

By scrutinizing Table 1 one can find: (a) While the LTO films grown on STO substrates show very small residual resistance $R(0)$, the value is slightly higher for NTO films on STO, and is the largest when both films are deposited on LAO substrates. It is known that the nominal hole concentration required to completely suppress the low-temperature AFM ordering increases with the correlation strength U/W[14]. Since the bandwidth
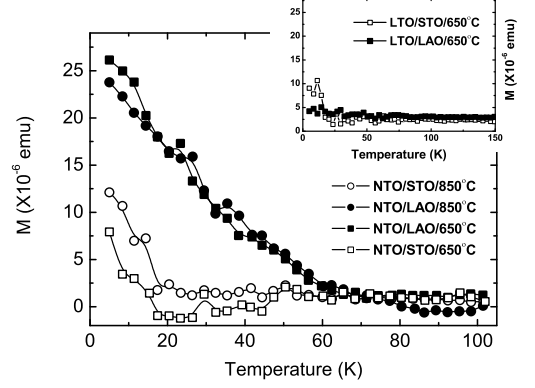
W in NTO is narrower than that in LTO and U in the two systems are equivalent, with similar doping, i.e. deposited in identical conditions, the AFM ordering still lingers in the NTO thin films, but dies in the LTO films, as clearly verified in Fig. 6. The figure also indicates that the NTO thin films grown on LAO substrates have a much higher T_N and a larger magnetic moment than the films grown on STO. This suggests that the former are " much more correlated ". Further research relevant to the substrate effect will be reported elsewhere later. The AFM ordering and fluctuations open an SDW gap on the Fermi surface, which decreases the Fermi surface area. The residual resistivity $R_s(0)$ is in inverse proportion to the Fermi surface area[15]. Thus the residual resistance lifts with increasing electron correlation strength. (b) The constant $C \sim A_\alpha \hbar^2/ne^2a^2t_p$ manifests its largest value in sample 140805, which was deposited in a higher oxygen pressure and concomitantly with a lower filling $n \approx 1 - \delta$. The second high value is found in sample 230505, a film grown on an LAO substrate. Intuitionally, C is roughly proportional to m^*/n, where m^* is the effective mass of polarons, and n is the carrier density. Apparently, polarons in the films on LAO possesses a larger m^* due to the higher correlation strength. One may note that, the heavily doped sample 241005 only exhibits an intermediate C, where the effect of its low n perhaps has been compensated by a remarkably reduced electron correlation, since the film is already away from the Mott-insulator-metal transition. (c) The characteristic temperature T_ω of the phonon coupled to electrons disperses in a scope from 97 to 374 K. This, however, disagrees with Gariglio's[10] argument that only a dominant optical phonon mode of $\hbar\omega_0/k_B = 80$ K contributes substantially to the resistivity. On the contrary, T_ω shows a weak dependence on the substrate materials. The phonon frequency for the films grown on STO tends to be higher than that on LAO. This may suggest a flaw in attributing the phonon simply to the tilt/rotation of

the oxygen octahedra in perovskite materials. The lattice mismatch strain between the films and the substrates may also play an important role, which directly affects the film lattice distortion, and thus the phonon. Further studies are required to clarify this issue.

IV. CONCLUSIONS

In summary, we have deposited LTO, NTO, and NSTO thin films on (100)STO and (100)LAO single crystal substrates by using the PLD technique. The oxygen pressure during deposition has been carefully controlled to ensure that the films are lightly hole doped near the metal-Mott-insulator boundary. The films are all epitaxially grown in a cube-on-cube way, and are metallic from room temperature to liquid helium. Their resistivity is T^2 dependent at high temperatures, but deviates from this law at temperatures below T^*. A temperature dependent Hall coefficient has also been observed. Therefore the films cannot fit in with the Fermi liquid frame. In spite of the fact that these films were prepared from different materials in varied deposition conditions, the temperature dependence of their resistivity can all be nearly perfectly fitted by a small-polaron coherent conduction model. In some of the films, at low temperatures a steep drop of the effective carrier density has been observed, which suggests an opening of the SDW gap due to the AFM spin fluctuations. Concomitantly the Fermi surface area decreases, so that these films have a relatively high residual resistance $R_s(0)$. Careful investigation on the fitting parameters implies that the substrates may have an important effect on the electron correlation strength in the films, and also on the frequency of the phonon coupled to the electrons.

* Electronic address: lijie@ssc.iphy.ac.cn
[1] M. Imada, A. Fujimori, and Y. Tokura, *Rev. Mod. Phys.* **70**, 1039(1998).
[2] Y. Fujishima, Y. Tokura, T. Arima, and S. Uchida, *Phys.Rev. B* **46**, 11167 (1992).
[3] Y. Tokura, Y. Taguchi, Y. Okada, Y. Fujishima, T. Arima, K. Kumagai, and Y. Iye, *Phys.Rev. Lett.* **70**, 2126(1993).
[4] M. J. MacEachern, H. Dabkowska, J. D. Garrett, G. Amow, Wenhe Gong, Guo Liu, and J. E. Greedan, *Chem. Mater.* **6**, 2092(1994).
[5] F. Lichtenberg, A. Herrnberger, K. Wiedenmann, J. Mannhart, *Progress in Solid State Chemistry* **29**, 1(2001).
[6] K. Kumagai, T. Suzuki, Y. Taguchi, Y. Okada, Y. Fujishima, and Y. Tokura, *Phys.Rev. B* **48**, 7636 (1993).
[7] A. Ohtomo, D. A. Muller, J. L. Grazul, and H. Y. Hwang, *Appl. Phys. Lett.* **80**, 3922(2002).
[8] A. Schmehl, F. Lichtenberg, H. Bielefeldt, and J. Mannharta, and D. G. Schlom, *Appl. Phys. Lett.* **82**, 3077(2003).
[9] J. W. Seo, J. Fompeyrine, H. Siegwart, and J.-P. Locquet, *Phys.Rev. B* **63**, 205401 (2001).
[10] S. Gariglio, J. W. Seo, J. Fompeyrine, J.-P. Locquet, and J.-M. Triscone, *Phys.Rev. B* **63**, 161103R (2001).
[11] G. M. Zhao, V. Smolyaninova, W. Prellier, and H. Keller, *Phys. Rev. Lett.* **84**, 6086(2000).
[12] M Isshiki, Y Fukudat and K Igaki, *J. Phys. F: Met. Phys.* **14** 3007(1984).
[13] D. B. McWhan, A. Menth, J. P. Remeika, W. F. Brinkman, and T. M. Rice, *Phys.Rev. B* **7**, 1920(1973).
[14] T. Katsufuji, Y. Taguchi, and Y. Tokura, *Phys.Rev. B* **56**, 10145(1997).
[15] Y. Taguchi, T. Okuda, M. Ohashi, C. Murayama, N. Mori, Y. Iye, and Y. Tokura, *Phys.Rev. B* **59**, 7917(1999).
[16] V. N. Bogomolov, E. K. Kudinov, and Y. A. Firsov, *Sov. Phys. Solid State* **9**, 2502(1968).